Influence of Ghost Lines on the Performance of Continuously Cast Special Structural Steels

F. FATTORINI, Centro Sviluppo Materiali, Roma, G. RONCHIATO, Centro Ricerche FIAT, Torino, M. BAFFIGI, D. DIGIANFRANCESCO, Nuova Deltasider, Milano, S. RIGONI, FIAT Auto, Torino

Abstract

An assessment was made of the in-use performance of special structural steels produced by the ingot and the continuous casting (c.c.) process. Particular attention has been paied to the influence of the ghost lines occasionally observed in c.c. products on the behaviour of mechanical components. Steel 40CrMo4 used by Fiat Auto for the manufacture of car front wheel hubs was studied in terms of its strength, ductility, low and high cycle fatigue resistence. Rotating bending fatigue tests were also performed on wheel hubs under simulated on-road conditions. A complete correspondence was observed between the metallurgical, static and dynamic properties of the steel produced by the two fabrication processes.

Riassunto

È stato eseguito un confronto tra acciai speciali da costruzione fabbricati con il ciclo da lingotto e quello da colata continua, valutando in particolare l'eventuale influenza delle "ghost lines", presenti saltuariamente nei prodotti da c.c., sulle proprietà di impiego dei componenti meccanici in esercizio. La sperimentazione è stata sviluppata sull'acciaio 40CrMo4, utilizzato dalla Fiat Auto per la fabbricazione di mozzi ruota anteriori per autovetture. Il confronto è stato eseguito sulla base delle proprietà resistenziali e di duttilità, della resistenza a fatica ad alto e basso numreo di cicli. Inoltre, sono state eseguite prove di fatica a flessione rotante direttamente su mozzi ruota, riproducendo le principali condizioni di esercizio su strada di tali componenti. La sperimentazione effettuata ha evidenziato la completa corrispondenza delle caratteristiche metallurgiche e meccaniche dei materiali prodotti con i due processi di fabbricazione.

1. Introduction

There has a gradual, but constant switch from lingot manufacture to continuous casting (c.c.) for the production of special steels in recent years.

None the less, there has been a measure of resistance to this change on the part of some users, particularly automakers, in the case of mechanical components regarded as critical with respect of in-service reliability and safety. This has been primarily generated by the occasional presence of ghost lines in c.c. products. These are observed in as-cast steel after macro etching in the form of dark interdendritic lines resembling cracks, and indeed often regarded as such until microstructural studies showed that they are not associated with discontinuity, and hence cannot be considered as cracks in the true sense. Another peculiar feature of ghost lines is that they are still clearly visible after thermomecanical treatments, such as rolling and forging.

Furthermore, there have been conflicting views on the real influence of ghost lines on the in-use performance of steels. Some workers are convinced that they constitue a defect in any event, an area of weakness in the material, even though no experiments have been specifically carried out in support of this opinion [1, 2], whereas other reports show that extensive experimentation has led to the opposite conclusion [3, 7].

The research described in this paper was conducted in conjunction by two research centres, a steel manufacturer, and a steel enduser. The aim has been to compare steels and components produced from ingots and c.c. billets. Particular attention is directed to determining the influence of ghost lines.

2. Materials

The steel investigated — 40CrMo4 — is produced by N. Deltasider, Turin (Italy), and is currently used by Fiat Auto for the manufacturing of a critical component, namely the front wheel hub of a widely sold car.

This steel is produced both in ingots and in 150 mm c.c. billets. A c.c. heat where ghost line were particulary evident, was selected. The chemical composition of the two steels is set out in Table 1. Some rolled ∅ 55 mm bars were also used to make wheel hubs at Teksid's Forging Division.

TABLE 1 - Per cent chemical composition of the ingot and c.c. steels

Process	C	Mn	Si	P	S	Ni	Cr	Mo	Cu	A1
c.c.	0.40	0.79	0.24	0.029	0.014	0.15	1.03	0.16	0.23	0.020
ingot	0.37	0.77	0.33	0.020	0.020	0.25	0.93	0.17	0.28	0.050

3. Experimental

Experiments were carried on both rolled bars and wheel hubs. Macrostructural, microstructural and microprobe investigations were made of the bars to obtain a better interpretation of the nature of ghost lines and hence acquire information concerning their origin. Extensive mechanical characterisation was undertaken in the laboratory by tensile tests and by low and high cycle fatigue tests; specimens were machined from bar areas with and without ghost lines.

Macro and micro structural investigations were also carried out on hubs to detect the presence of ghost lines and their position in relation to the critical zones, i.e. those subjected to stess concentration.

Rotatory bending fatigue tests simulating real on-road conditions were performed on hubs made from ingot and c.c. steel.

Electron microscopy and microfractogrophy were used to locate fatigue crack initiations and determine their possible correlations with the presence of ghost lines.

4. Results and discussion

4.1 Rolled bars

4.1.1 Macro, microstructural and microprobe investigations

Cross-sections of the rolled bars after macro etching are illustrated in the photos in fig. 1. Ghost lines are clearly visible as thin, short, dark marks starting a few millimetres below the surface and penetrating inwards.

From a microstructural point of view they may be considered as discontinuities. In the as-rolled specimens, these consist of variously extensive martensite areas buried in a bainite matrix, sometimes associated with alignments of nonmetal inclusions mostly composed of manganese sulphides. Their microstructural appearance closely resembles that observed in the central area of the bar, which is influenced by axial segregation (fig. 3). Ghost lines are still visible after quenching and tempering (fig. 4). Their hardness is constantly higher, averaging some 100 HV more than the base material, both in the as-rolled and quenched and tempered condition (Table 2). Microanalysis of ghost lines obtained by an EPMA microprobe using a ∅ 5 μ spot showed local concentration in impurities and alloy elements similar to those found in the central segregation in agreement with the microstructural picture. As shown in tab. III this was particularly evident for P (up to 10 times more than in the matrix), Mo (up to 2.7 times), S (up to 2.3 times), C (up to 1.6 times) and Cr (up to 1.8 times).

These results suggest that ghost lines are formed in the following way. During the initial solidification of the c.c. grillet, thermal and/or mechanical stresses, combined with reduced strength of the solidified

shell, may create tiny cracks in the liquid-solid interface, are immediately filled by the liquid steel nearby. As soon as the solidification front shifts inwards as cooling proceeds, these cracks — which are still full of liquid steel — may remain isolated and hence give rise to small pockets completely surrounded by solid steel. An independent solidification process thus takes place in their interior with its own segregation phenomena. The last portions of material to solidify are obviously those with the highest segregating element concentrations. The chemical composition varies locally, the segregation elements alter the hardenability and during cooling results in the discontinuities observed at macro- and microstructural are level.

TABLE 2 - Hardness values (HV_{20g}) in the matrix and ghost lines in the as-rolled and quenched and tempered conditions

As-rolled				Quenched & Tempered(1)			
Matrix		Ghost Lines		Matrix		Ghost Lines	
x	s	x	s	x	s	x	s
291	20	371	53	283	9	406	26

(1) Austenitization 860°C × 1/2 h
Oil quenching
Subcritical annealing 620°C × 2 h
x = mean values for 25-60 hardness measures on various specimens
s = Standard Deviation

TABLE 3 - Concentrations of alloy elements and impurities in the ghost lines as measured with a EPMA microprobe

Point of measurement	C	Si	P	S	Mo	Cr	Mn
Matrix	0.381	0.428	0.036	0.020	0.25	1.164	0.797
Ghost lines E.I.*	1.6	1.5	10	2.3	2.7	1.6	1.3
Central segregation E.I.*	1.5	1.4	12	2.0	4.0	1.8	1.4

(*) Concentration index: ratio between ghost line and matrix values

4.1.2 Mechanical properties

Tests were run on quenched and tempered material. The heat treatment conditions were those normally used for the wheel hubs in question, namely:

— austenitization: T = 860°C × 1/2 hr

— quenching: immersion in stirred oil at T = 50°C

— tempering: T = 620°C × 2 hr.

The results of the tensile tests are shown in Table IV. It can be seen that the presence of ghost lines has no significant effect strength (UTS and σ_γ), ductility (E_5) and reduction in area (RA), and suitability for strain-hardening exponent (n) and strength coefficient (K).

Similar results were obtained by the high cycle fatigue tests. The fatigue limit (measured by the "staircase" method) was 776 MPa (SD 56 MPa) and 768 MPa (SD 26 MPa) for the specimens without

and with ghost lines respectively (figs. 5, 6). The tests were performed by subjecting the specimens to tensile fatigue test with stress ratio R = 0,05 and frequency of 350 Hz. This method ensures uniform stress distribution over the section of the test specimen. It was preferred to the rotating bending fatigue test because it can reveal any influence due to the presence of all the ghost lines and not only those reaching the surface, whereas only the latter would be investigated by the other test, since it subjects the specimen to bending stresses cyclically.

The results obtained in the low-cycle fatigue tests are shown in figs. 7 and 8. These tests were carried out on tensile specimens in strain control mode at a frequency of 1 Hz. The total absence of influence of the ghost lines is evident by the virtual coincidence of the true stress-true strain (fig. 7) and the Manson-Coffin curves $\Delta\varepsilon_{t/2} = f\ (2N_f)$ (fig. 8).

TABLE 4 - Tensile propectics

Specimen	UTS (MPa)		σ_γ (MPa)		E_5 (%)		RA (%)		n		K (MPa)	
	x	s	x	s	x	s	x	s	x	s	x	s
With ghost lines	1090	3	937	3	16.3	0.5	60	1.3	0.079	0.006	1352	26
Without ghost lines	1088	4	934	5	16.4	0.3	60	1.6	0.074	0.010	1369	10

x = mean
s = S.D.

4.2 Wheel hubs

4.2.1 Macro and microstructural examinations

Wheel hubs were macro etched, sectioned longitudinally and examined to see whether ghost lines were also present on the components. As can be observed in fig. 9, they are clearly visible and thus retain their identity even after hot forging.

They are situated 2-3 mm on average below the outer surface of the hub in keeping with their relative closeness to the surface in the as-cast material and in the rolled bar. At their microstructural level ghost lines mountain their characteristic appearance (fig. 10), and present local hardness increments of about 100 HV as already observed in the rolled bar. None the less, this increase in hardness was never accompanied by internal defects in the numerous specimens examined, even when ghost lines were present in hub areas subjected to plastic deformation during forging. The conclusion may thus be drawn that they do not have a significant incidence on the hot ductility of the material.

4.2.2 Fatigue tests

4.2.2.1 Test method

Since it was impossible to carry out test under the real conditions in which a wheel hub operates, a rotating bending set-up was prepared to simulate the main fatigue conditions (fig. 11). Rotating bending was simulated by three servohydraulic actuators placed at 120° to each other. A rotating force Fo was simulated by applying to each jack a sinusoidal dynamic force equivalent to 2/3 Fo and a phase offset of $2/3\pi$.

To take into account the possible occurrence of a wheel bumping against the pavement, the load was applied with an angle of 34°45′ to the road surface (fig. 12); this condition reproduces that used by Fiat

Auto during its bench tests. The reference load (Fo) was 6600 ± 6500 N, in which the static component served to operate each branch in traction only, while the dynamic component, since the effect of the three branches was combined through spatial orientation and phase offsets, generated the rotating bending moment.

To prevent unwarrented failure of the bearing, since it is required to operate at a fixed point instead of in rotation in accordance with its specific duty condition, it was therefore replaced by a bush.

This decision was legittimated by making sure that it did not result in any appreciable change in the state of strain on the critical areas of the hub.

For this purpose, a hub was instrumented with strain gauges (figs. 13, 14) along two opposite generatrixes at the five fillets (Nos. 1-5 in fig. 15) regarded as the most critical zones for fatigue failures.

A bearing was then mounted on the instrumented hub. Static load of up to 5000 N were applied and the strain gauge values recorded. The test was then repeated with a bush instead of a bearing.

Comparison of the results in Table V shows that the greatest stress was exerted at fillet 3 and that the strain pattern was much the same for the two arrangements.

As expected, the only difference of any significance was observed for fillet 4, where application of the bush resulted in an approximately 30% reduction in load sensitivity. However, when it is remembered that the state of strain of this fillet is about 75% of that of the most critical one (No. 3) when a bearing is mounted, this reduction in sensitivity can be regarded as negligible, particularly in a comparative assessment of the fatigue behaviour of the hub.

TABLE 5 - Calibration of the test system and comparison between the set-up with a bearing and that with a bush. The deformation values are the means of those recorded for the two generatrixes

Stain gauge N.	Set up		Bush/Bearing
	Bearing (με)	Bush (με)	Ratio
1	670	649,5	0,97
2	865	718,5	0.83
3	2098	2152,5	1.03
4	1553.5	1087	0.70
5	896	876	0.98

4.2.2.2 Results

The tests set out to characterise ingot and c.c. steel wheel hubs in tems of Wöhler curve up to and beyond the cut-off point.

The results are shown in fig. 16. Where the forces are in percentages of Fo and life to failure in numbers of cycles. It is clear that the data for the c.c. steel hubs are similar to those carried out on ingot steel and are also less scattered. This phenomenon is all the more the apparent the higher the loads and hence the earlier the failure.

The fatigue limit was determined using the "staircase" method, with the life fixed at 5.10^6 cycles. This high value was chosen to ensure precautionary results in view of the obvious strategic importance of a wheel hub to the reliability and safety of a road vehicle. Halfway through the test, the hubs were

removed and examined by a magnetoscope to detect the presence of fatigue crack initiation points. The analysis was repeated each time appropriate instrumentation revealed a difference between the current load wave and the initial one.

The staircase results for the c.c. steel and ingot steel hubs are shown in figs. 17 and 18 respectively. Once again, no significant differences emerge, though it may be noted that the c.c. steel had a slightly higher 50% probability of survival fatigue limit (88% versus, 83% of Fo), with, however, a wider dispersion (20% Fo versus 8% Fo).

4.2.3 Fractographic analyses

Even though the strength and fatigue tests had shown that the production process was not an influential factor, it was decided to carry out an extensive fractographic study (SEM-EDAX) of the fracture surfaces of the test specimens and hubs, to see whether ghost lines act as the preferential local condition for cracks initiation, and hence have a real effect on the service life of a component.

As shown in figs. 19 & 20, a ghost line was identified on one of the specimens used in the tensile tests. It took the form of a local variation of the fracture micromechanism, from ductile in the matrix to low-energy microductile on the ghost line, where some MnS inclusions were also detected. None the less, the fracture was not influenced by the presence of the ghost lines or inclusions in either the crack initiation or propagation.

Nothing that could be attributed to ghost lines were detected in any of the other specimens used for the tensile and high- and low-cycle fatigue tests.

The same was true of the wheel hubs. Fractures took place without the evident influence of "weakened" areas. A multiple points fatigue crack initiation is observed (fig. 21) starting from the outer surface of the hub, generally located at fillet no. 3, where the strain gauge analysis showed the maximum stress concentration. The inclusions at this point were primarily composed of aluminates and/or silicon aluminates (fig. 22), instead of to MnS, which could have been correlated to the presence of ghost lines.

5. Conclusions

The following conclusions can be drawn from this extensive series of experiments and studies carried out on ingot and c.c. 40CrMo4 steel bars and wheel hubs to determine the nature and origin of ghost lines, and their possible influence on the performance of hubs in service:

1) In the as-rolled bars, ghost lines take the form of microstructural discontinuities consisting of martensitic zones immersed in a totally bainitic matrix. They are often associated with inclusion alignments composed of manganese sulphides. They can still be distinguished from the matrix after quenching and tempering, albeit within a more uniform microstructure of subcritically annealed martensite. Microprobe analysis revealed segregation impurities (particularly P, Mo, S, C and Cr) in the ghost lines. In addition, their hardness was about 100 HV greater than that of the matrix on average.

2) The most likely explanation of the way ghost lines are formed is that during solidification of the c.c. matrix small cracks are created in the liquid-solid interface and immediately filled by the surrounding liquid. As the solidification front advances, these pockets of liquid solidify independently, resulting in segregation phenomena in their interior. Through their local alteration of the chemical composition of the base steel, these segregations give rise to the microstructural discontinuities and variations in hardness observed in this study.

3) Strength tests carried out on specimens showed that ghost lines have no influence on strength and ductility, suitability for work-hardening, and resistance to high and low-cycle fatigue. No coincidence was ever observed between ghost lines and the multiple points crack initiation of fatigue failure.

4) The rotating bending fatigue tests performed on the hubs with modalities simulating actual service conditions also made it clear that ghost lines are without influence. This was demonstrated both by the low cycle and by the high-cycle fatigue tests. As for the test specimens, a thorough microstructural and microfractographic investigation confirmed the absence of any correlation between ghost lines and the location of the fatigue crack initiation.

Figure captions

Fig. 1: Cross-sections of the rolled bars after macro etching.

Fig. 2: Ghost line on as-rolled 40CrMo4 steel. 2% Nital etching.

Fig. 3: Microstructure of central segregation. 2% Nital etching.

Fig. 4: Ghost line on quenched and tempered specimen. 2% Nital etching.

Fig. 5: Results of high-cycle fatigue tests on specimens "without" ghost lines (R = 0,05). Fatigue limit x = 776 MPa (S.D. = 56 MPa).

Fig. 6: As last: specimens "with" ghost lines. Fatigue limit x = 768 MPa (S.D. = 26 MPa).

Fig. 7: Low-cycle fatigue tests. Cyclic curves obtained on materials "with" and "without" ghost lines and comparison with the monotonic "true stress - true strain" curve.

Fig. 8: Comparison between Manson-Coffin curves for materials "with" and "without" ghost lines.

Fig. 9: Longitudinal section of a wheel hub after macro etching.

Fig. 10: Ghost lines on a wheel hub.

Fig. 11: Experimental rig for fatigue tests on wheel hubs.

Fig. 12: Loading condition used for the wheel hub fatigue tests. The load direction is at an angle to the vertical to take account of accidental effects, such as those imposed when a wheel hits the pavement.

Fig. 13: Layout of the strain gauges on the upper part of the hub.

Fig. 14: Layout of the strain gauges on the lower part of the hub.

Fig. 15: Location of the strain gauges in relation to the five critical fillets.

Fig. 16: Results of fatigue tests on wheel hubs.

Fig. 17: Results of staircase fatigue tests on wheel hubs made from c.c. steel. Fatigue limit m = 88% Fo (S.D. = 20% Fo).

Fig. 18: As last: wheel hubs made from ingot steel. Fatigue limit m = 83% Fo (S.D. = 8% Fo).

Fig. 19: Ghost line on fracture surface of a tensile test specimen.

Fig. 20: Detail of fig. 19.

Fig. 21: Fatigue crack initiation points at fillet no. 3 on wheel hubs made from c.c. steel.

Fig. 22: Ca aluminate inclusions in fatigue crack initiation areas on wheel hubs made from c.c. steel.

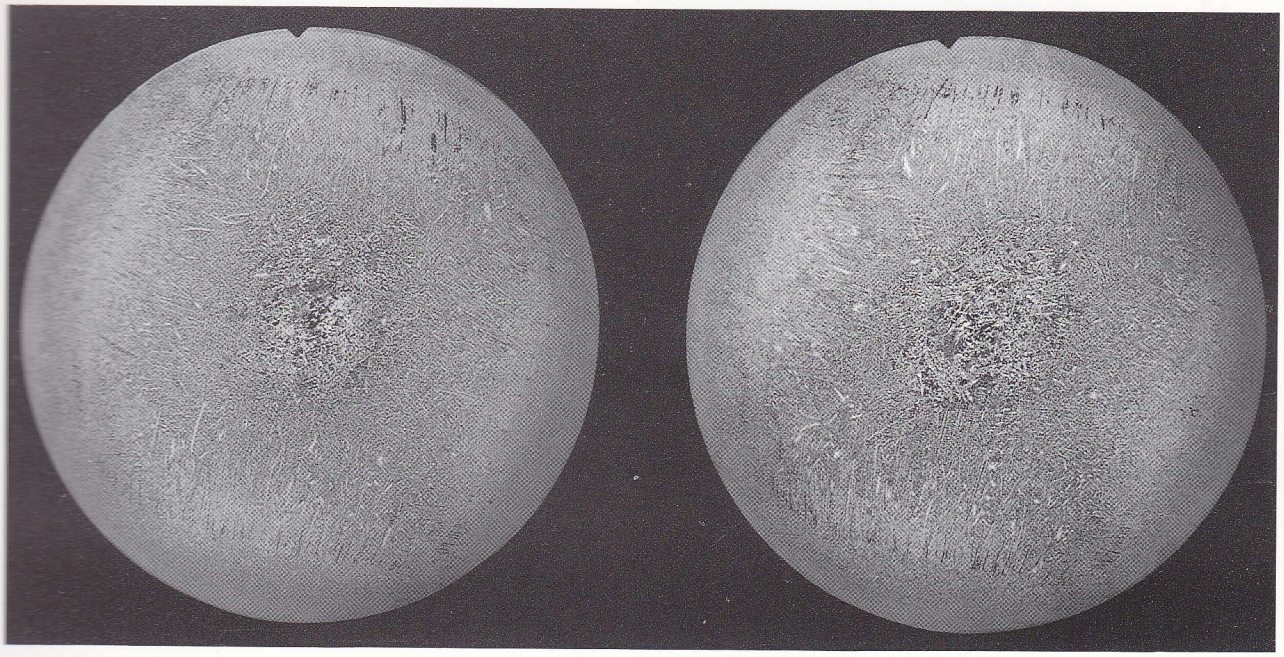

Fig. 1

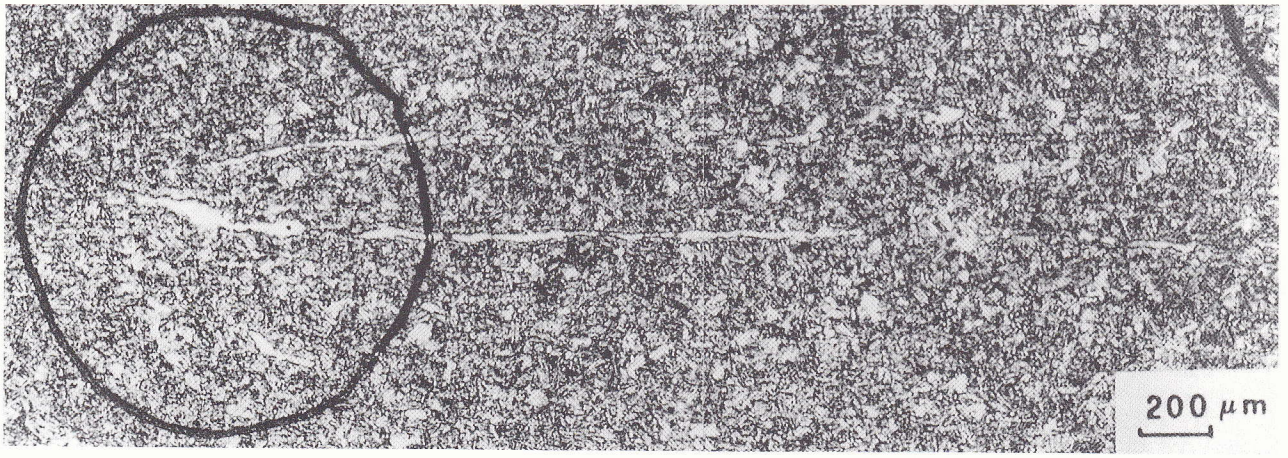

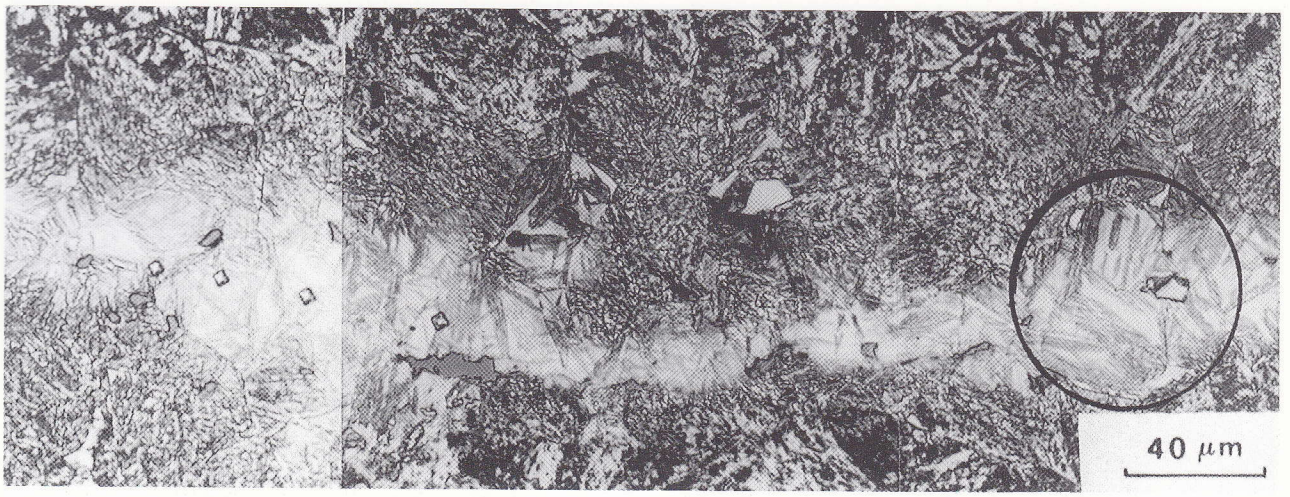

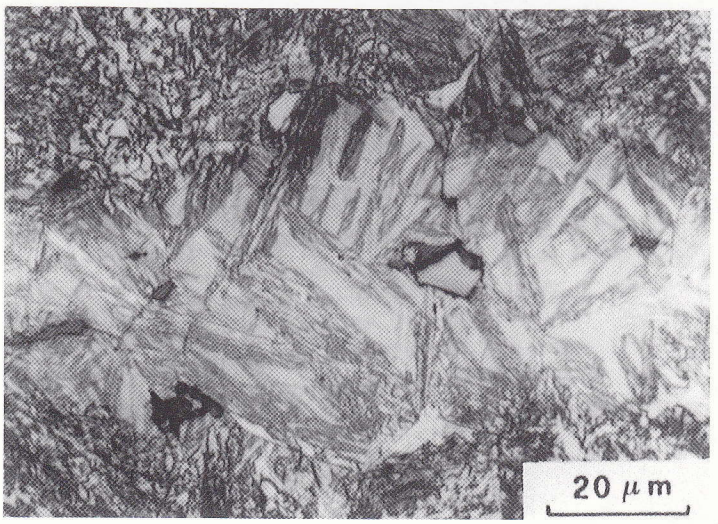

Fig. 2

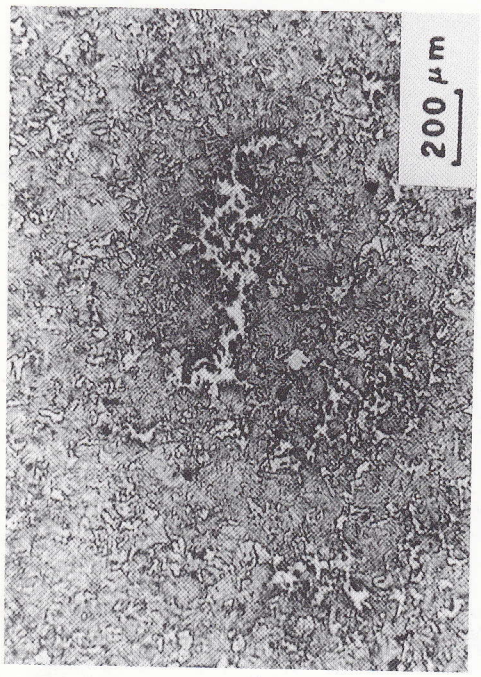

Fig. 3

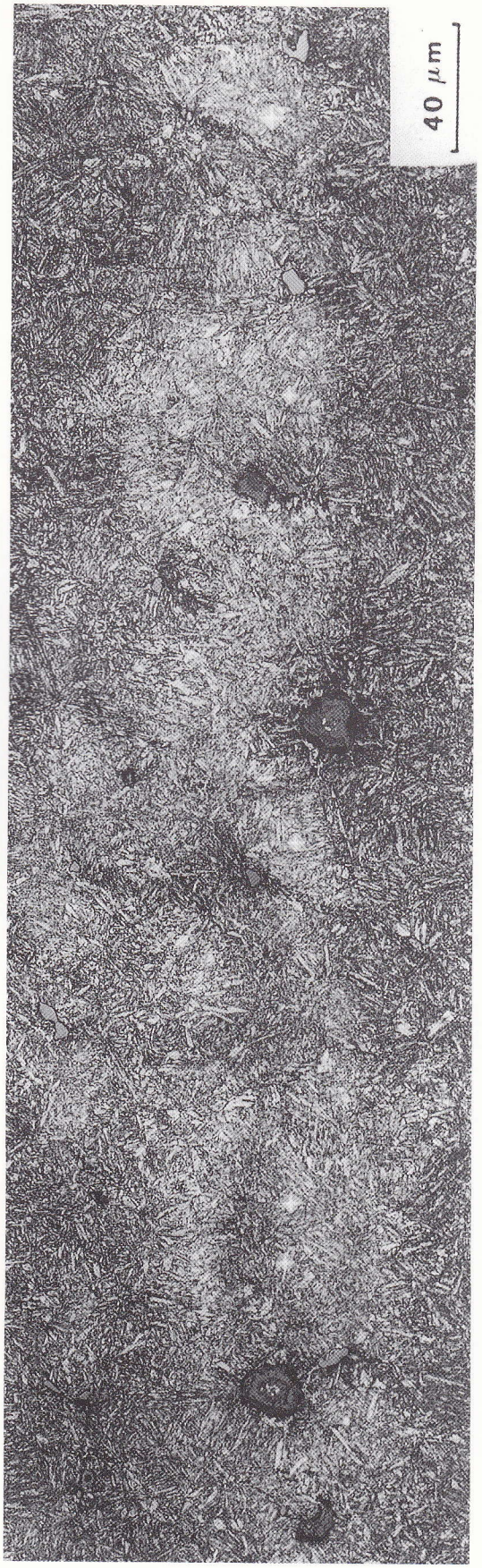

Fig. 4

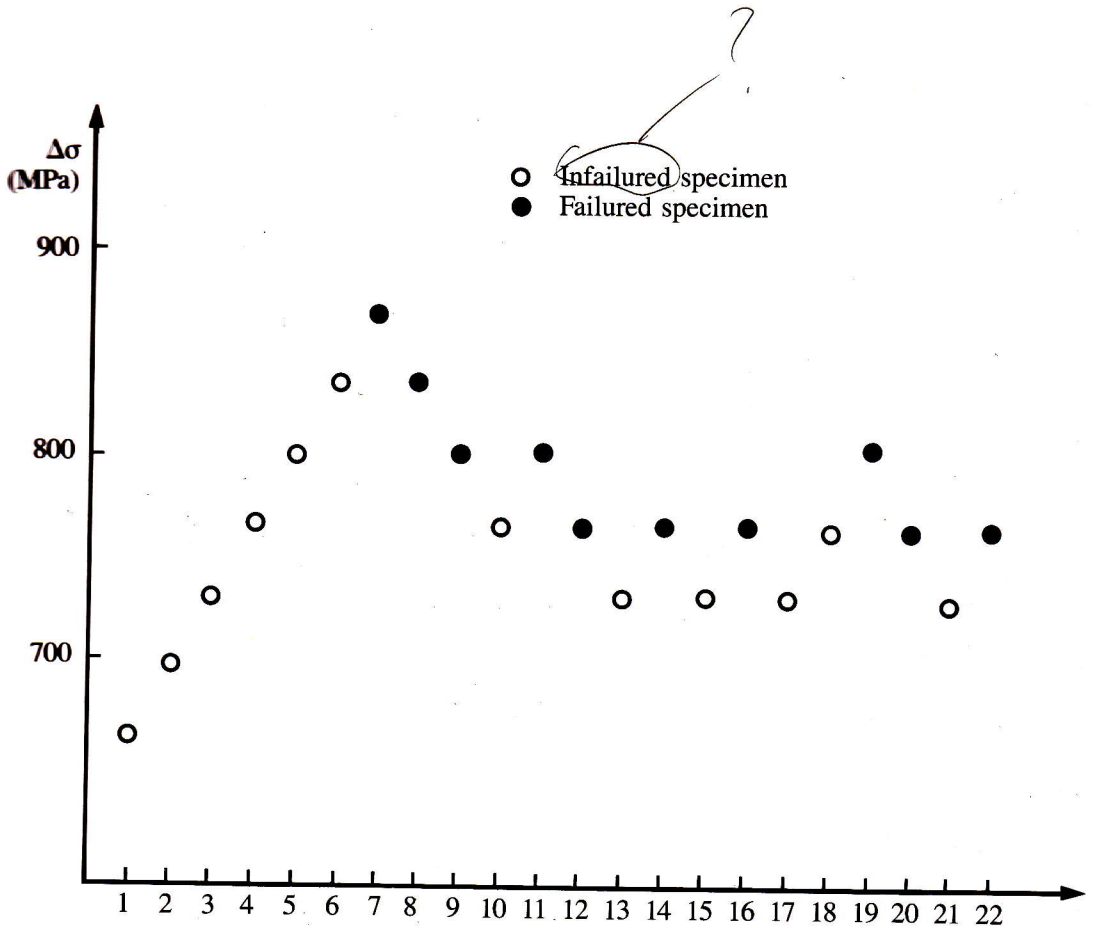

Δσ (MPa)	i	n_i ROTTE	$i \cdot n_i$	$i^2 \cdot n_i$
871	3	1	3	9
836	2	1	2	4
801	1	3	3	3
766	0	5	0	0
		N = 10	A = 8	B = 16

$$\overline{x} = x_o + x \left(\frac{A}{N} \pm \frac{1}{2}\right) = 776 \text{ MPa}$$

$$\sigma = 1.62 \cdot x \left(\frac{NB - A^2}{N^2} + 0.029\right) = 56 \text{ MPa}$$

Fig. 5

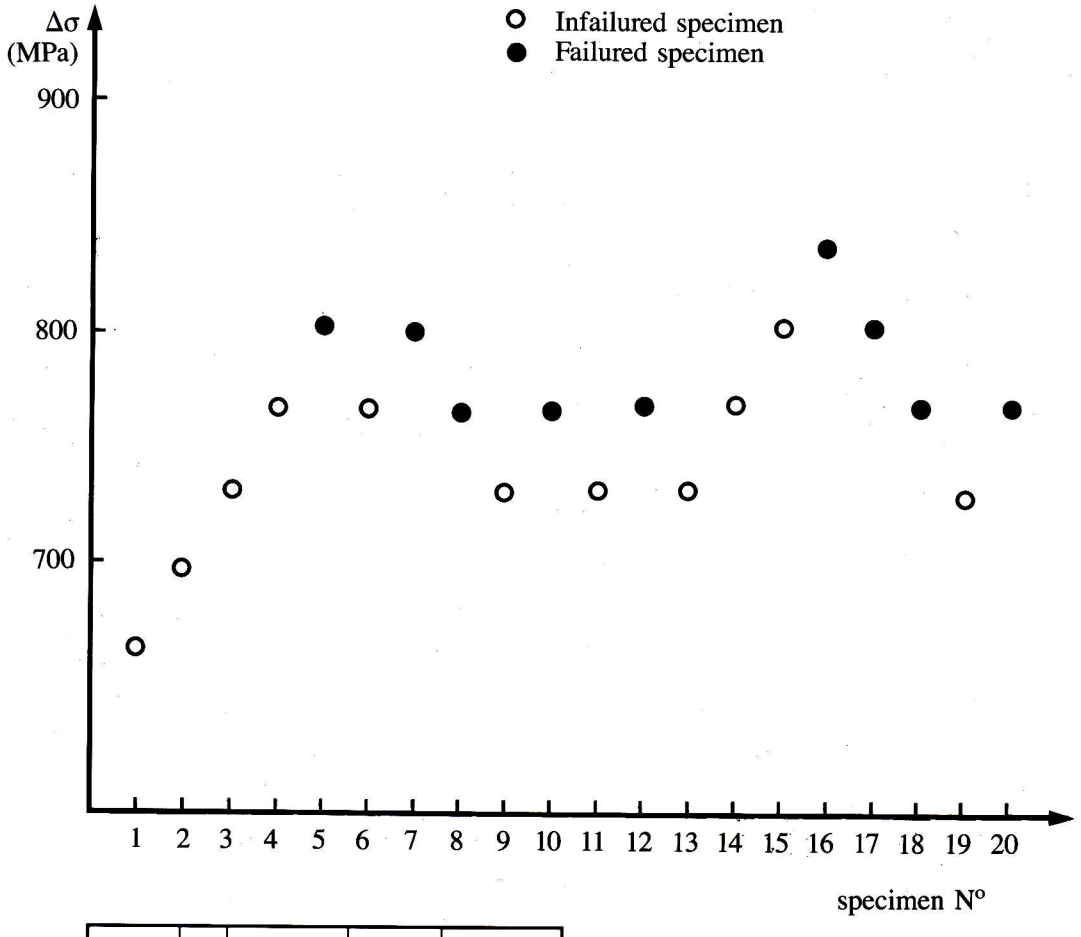

Δσ (MPa)	i	n_i ROTTE	$i \cdot n_i$	$i^2 \cdot n_i$
836	2	1	2	4
801	1	3	3	3
766	0	5	0	0
		N = 9	A = 5	B = 7

$$\overline{x} = x_o + x \left(\frac{A}{N} \pm \frac{1}{2}\right) = 768 \text{ MPa}$$

$$\sigma = 1.62 \cdot x \left(\frac{NB - A^2}{N^2} + 0.029\right) = 26 \text{ MPa}$$

Fig. 6

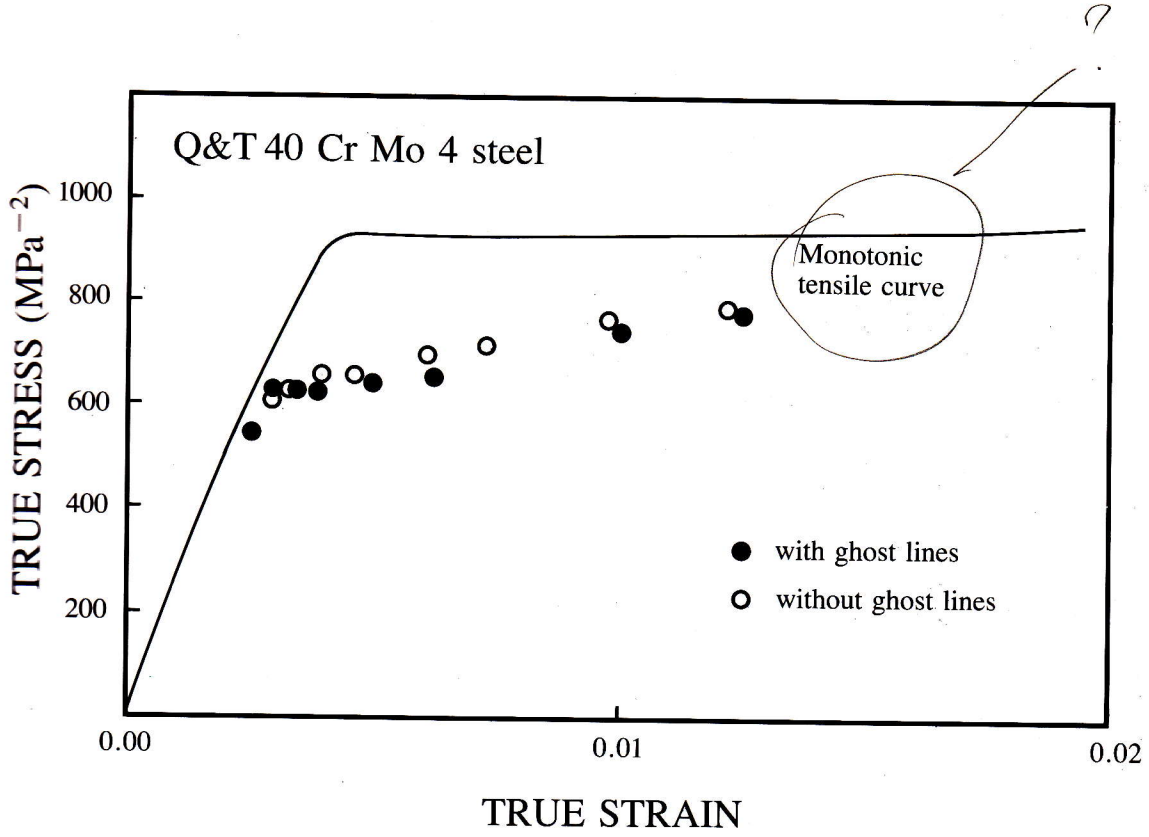
Q&T 40 Cr Mo 4 steel
TRUE STRESS (MPa^{-2})
1000
800
600
400
200
0.00
0.01
0.02
TRUE STRAIN
Monotonic tensile curve
with ghost lines
without ghost lines

Fig. 7

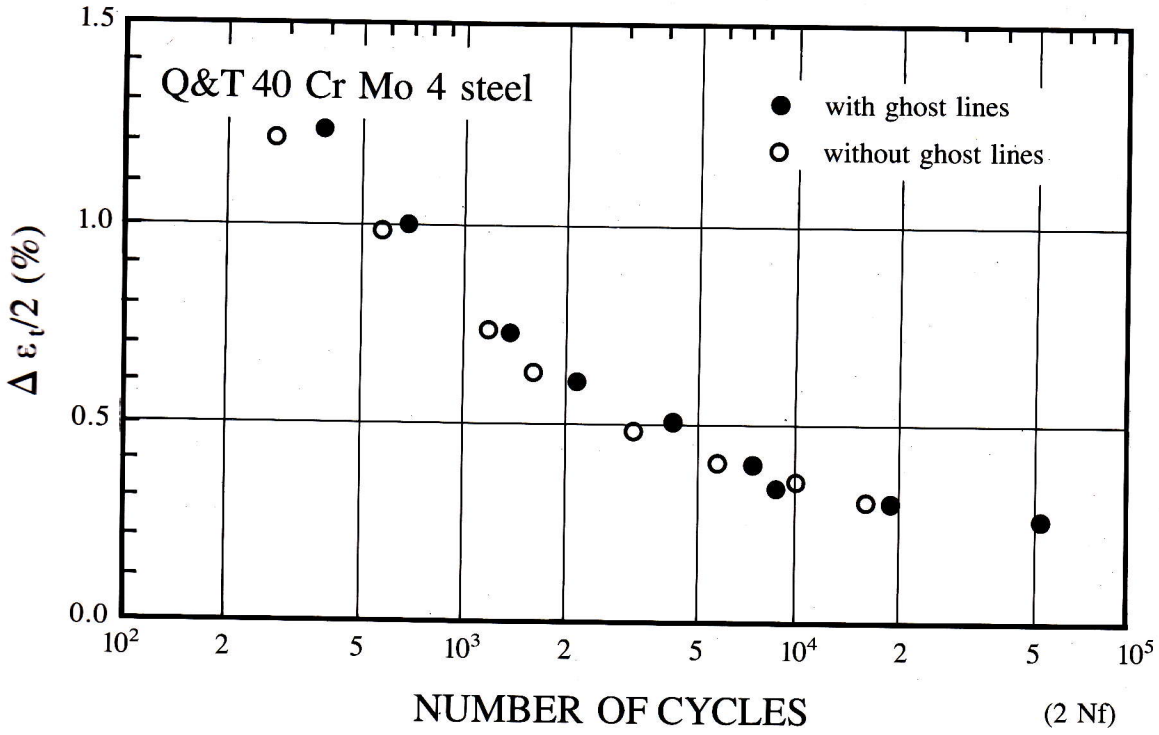
Q&T 40 Cr Mo 4 steel
$\Delta \varepsilon_t/2$ (%)
1.5
1.0
0.5
0.0
10^2
2
5
10^3
2
5
10^4
2
5
10^5
NUMBER OF CYCLES
(2 Nf)
with ghost lines
without ghost lines

Fig. 8

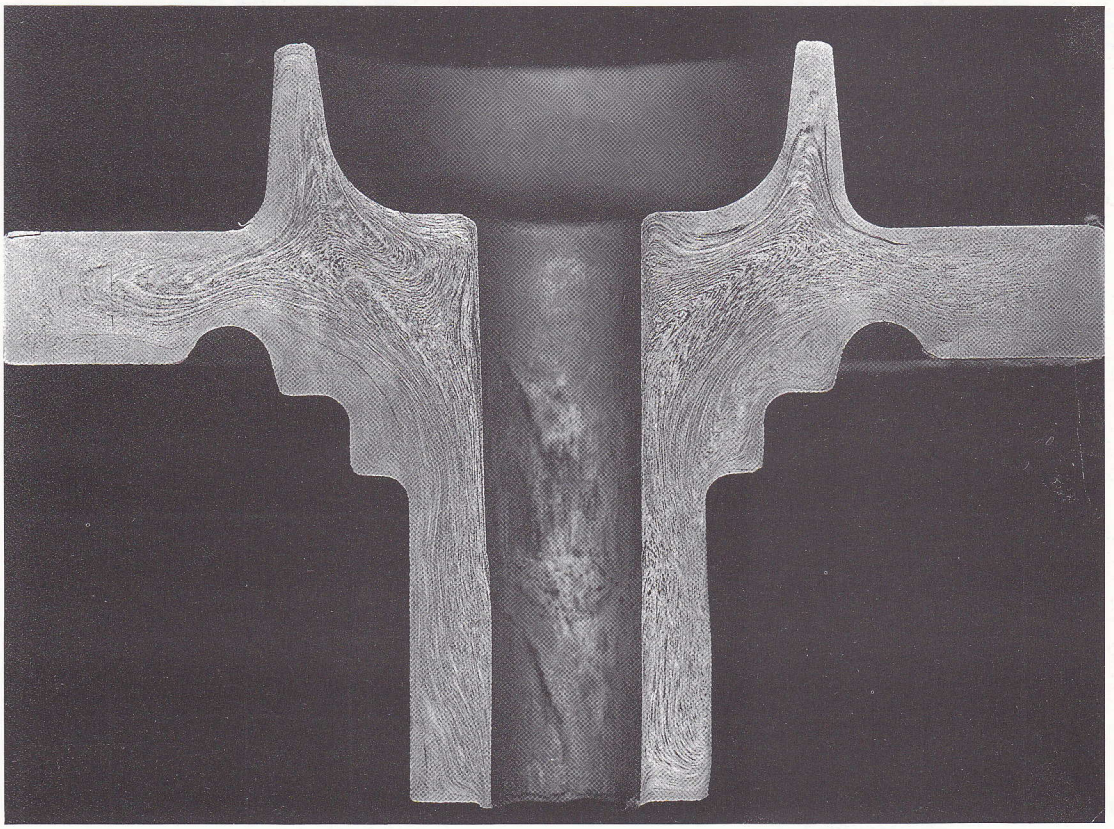

Fig. 9

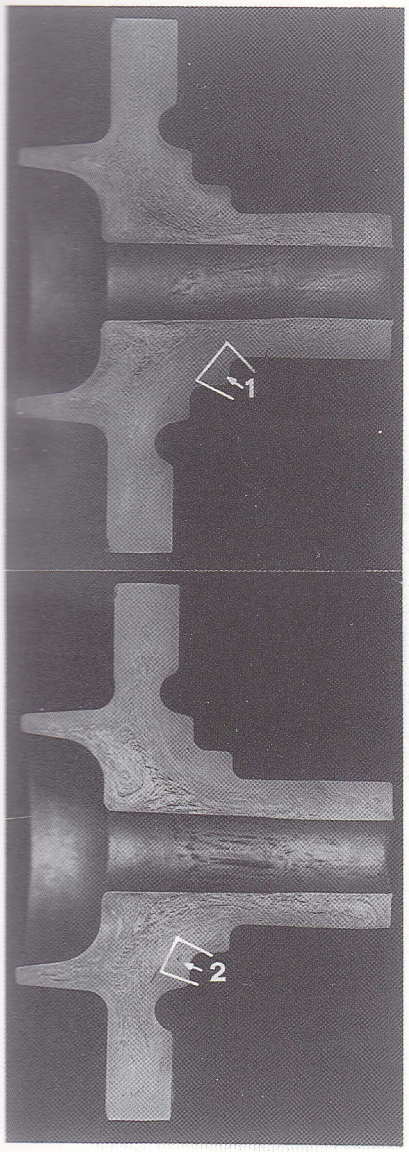

HCl 50% etching

WHEEL HUBS No. 2 and No. 3.

1

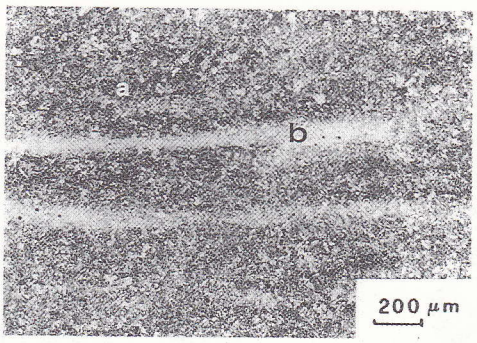

a: microhardness 260 HV_{20g}

b: " 350 HV_{20g}

2

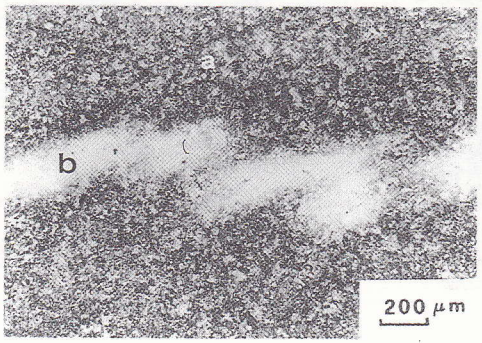

a: microhardness 260 HV_{20g}

b: " 340 HV_{20g}

Fry etching

Fig. 10

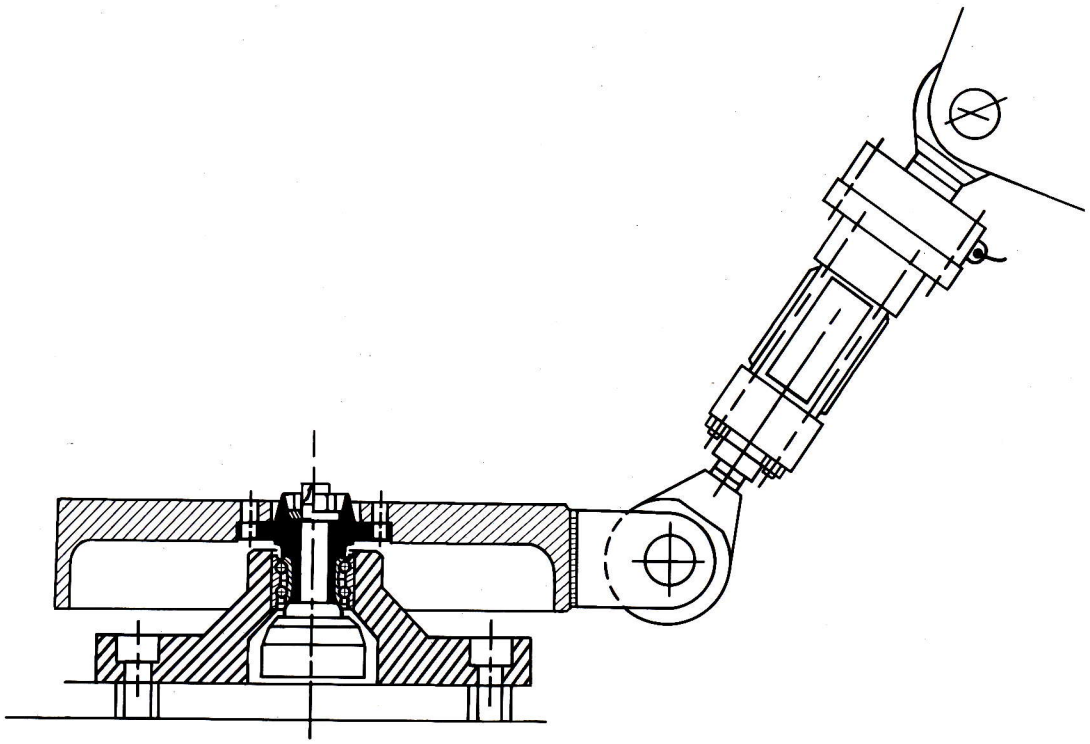

Fig. 11

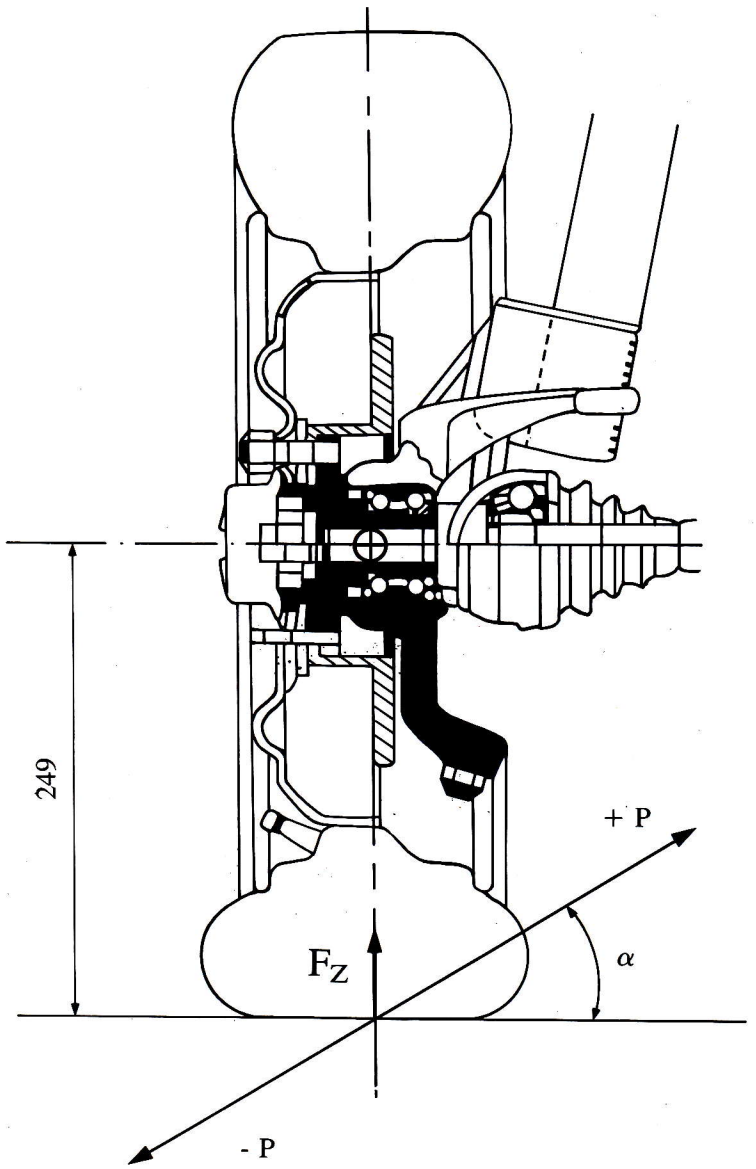

Fig. 12

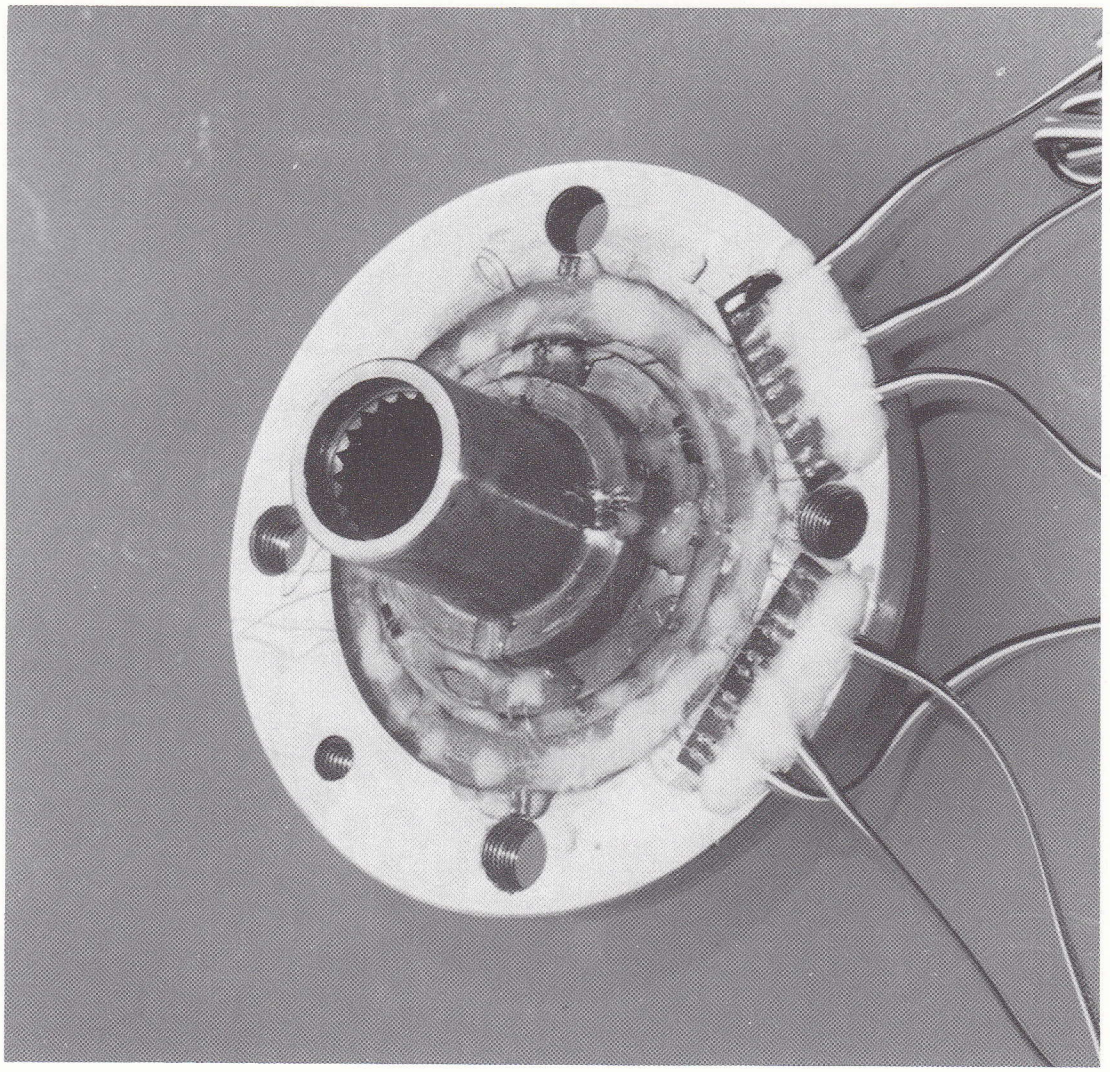

Fig. 13

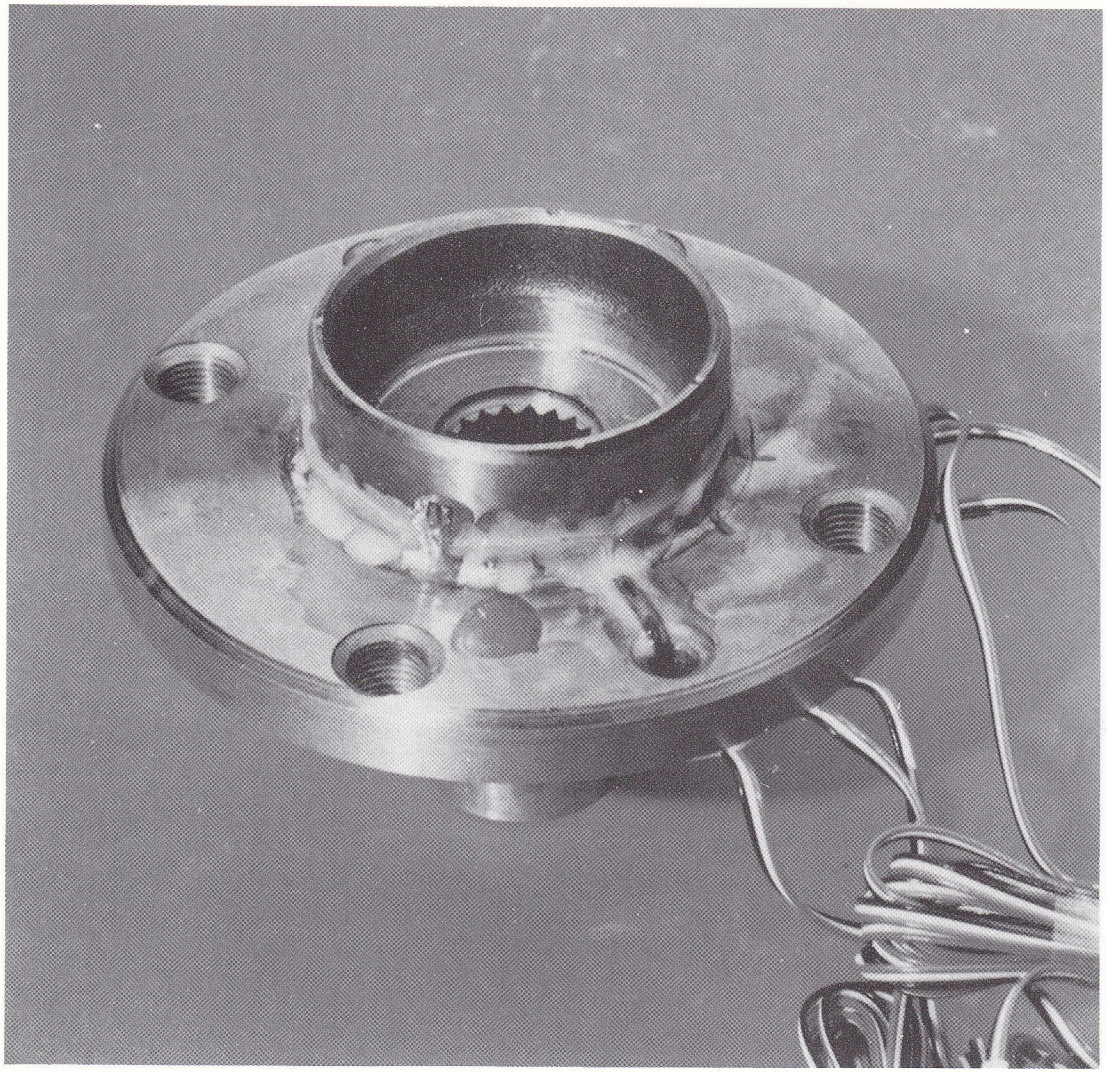

Fig. 14

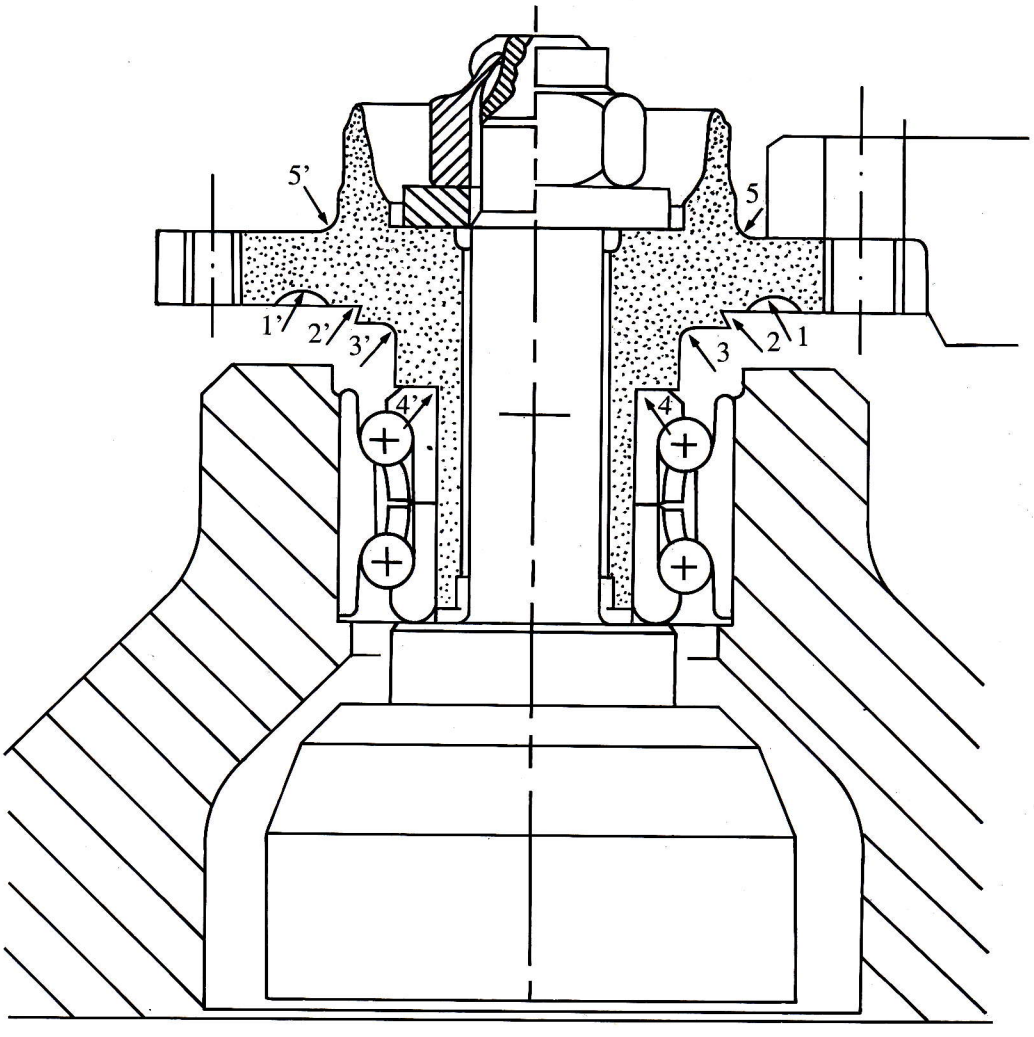

Fig. 15

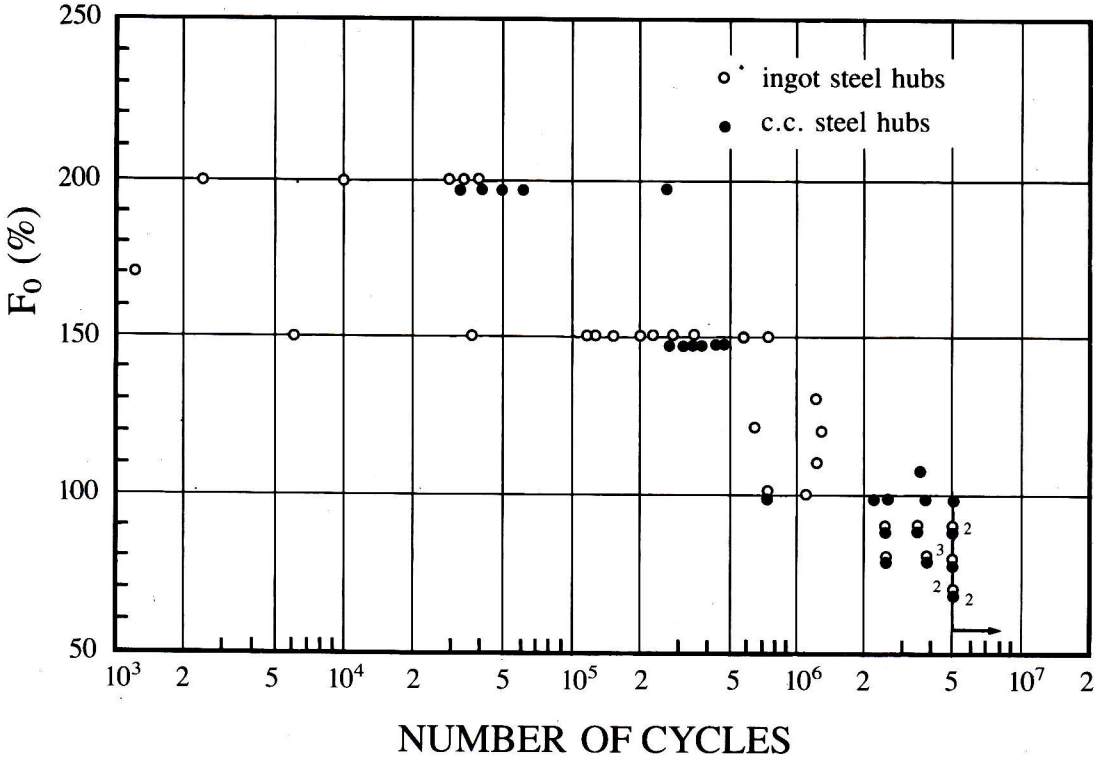
250
200
150
100
50
F_0 (%)
ingot steel hubs
c.c. steel hubs
10^3 2 5 10^4 2 5 10^5 2 5 10^6 2 5 10^7 2
NUMBER OF CYCLES

Fig. 16

Liv.	Fi	ORDINE DELLE PROVE																				Nº di prove	
I	% Fo	1	2	3	4	5	6	7	8	9	10	11	12	13	14	15	16	17	18	19	20	×	O
4	110				×																	1	
3	100	×		O		×		×														3	1
2	90		O				O		×						×							2	2
1	80									×		×		O		×						3	1
0	70										O		O									0	2
Nº di cicli	× 10⁶	.759	5.	5.	2.5 ÷ 5	2.5 ÷ 5	5.	< 2.5	< 2.5	2.5 ÷ 5	5.	3.85	5.	5.	3.45	< 2.5						Σ = 9	Σ = 6
																						r_i	i_I

N_i	I	$I \times N_i$	i^2	$i^2 \times N_i$
1	3	3	9	9
2	2	4	4	8
1	1	1	1	1
2	0	0	0	0
N = 6		A = 8		B = 18

$N = r_i$ per $\Sigma r_i < \Sigma I_i$ (caso1)
$N = I_I$ per $\Sigma r_i \geq \Sigma I_i$ (caso2)

d = 10% Fo
X = rotta
O = non rotta

CASO 1: $m = d\left(\frac{A}{N} - 0{,}5\right) + F_{I=0}$

CASO 2: $m = d\left(\frac{A}{N} + 0{,}5\right) + F_{I=0}$

m = 88% Fo

$S = 1{,}62\ d\left(\frac{NB - A^2}{N^2} + 0{,}029\right)$

S = 20% Fo

Fig. 17

Liv.	Fi	ORDINE DELLE PROVE																				Nº di prove	
I	% Fo	1	2	3	4	5	6	7	8	9	10	11	12	13	14	15	16	17	18	19	20	×	O
6	130	×																				1	
5	120		×																			1	
4	110			×																		1	
3	100				×		×															2	
2	90					O		×		×						×						3	1
1	80								O		×		×		O		O					2	3
0	70											O		O								0	2
Nº di cicli	× 10⁶	1.223	1.294	1.262	1.107	5.	.740	2.542	5.	< 2.5	2.5 ÷ 5	5.	2.5 ÷ 5	5.	5.	3.5	5.					Σ = 10	Σ = 6
																						r_i	i_I

N_i	I	$I \times N_i$	i^2	$i^2 \times N_i$
1	2	2	4	4
3	1	3	1	3
2	0	0	0	0
N = 6		A = 5		B = 7

$N = r_i$ per $\Sigma r_i < \Sigma I_i$ (caso1)
$N = I_I$ per $\Sigma r_i \geq \Sigma I_i$ (caso2)

d = 10% Fo
X = rotta
O = non rotta

CASO 1: $m = d\left(\frac{A}{N} - 0{,}5\right) + F_{I=0}$

CASO 2: $m = d\left(\frac{A}{N} + 0{,}5\right) + F_{I=0}$

m = 83% Fo

$S = 1{,}62\ d\left(\frac{NB - A^2}{N^2} + 0{,}029\right)$

S = 8% Fo

Fig. 18

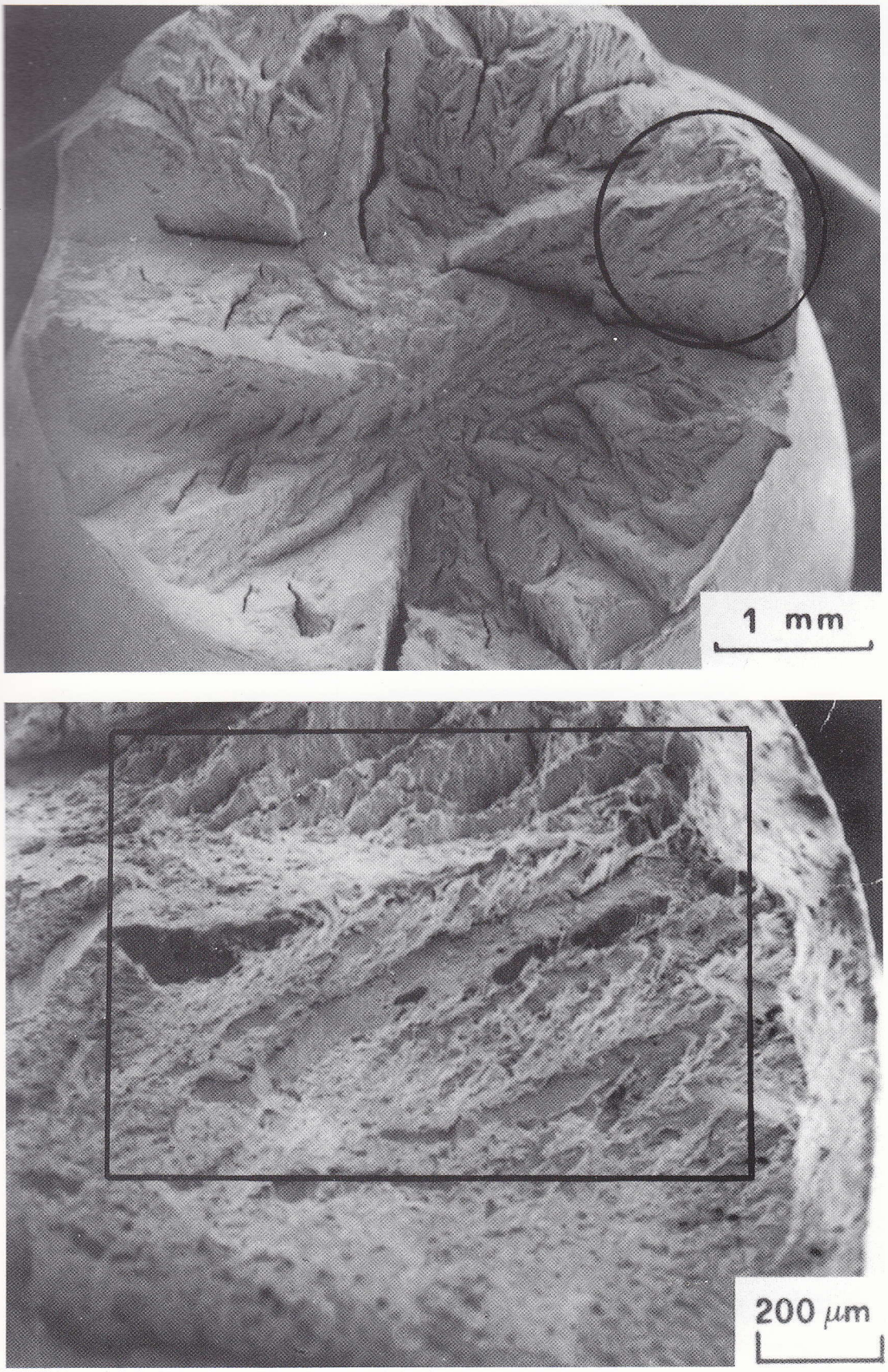

Fig. 19

Fig. 20

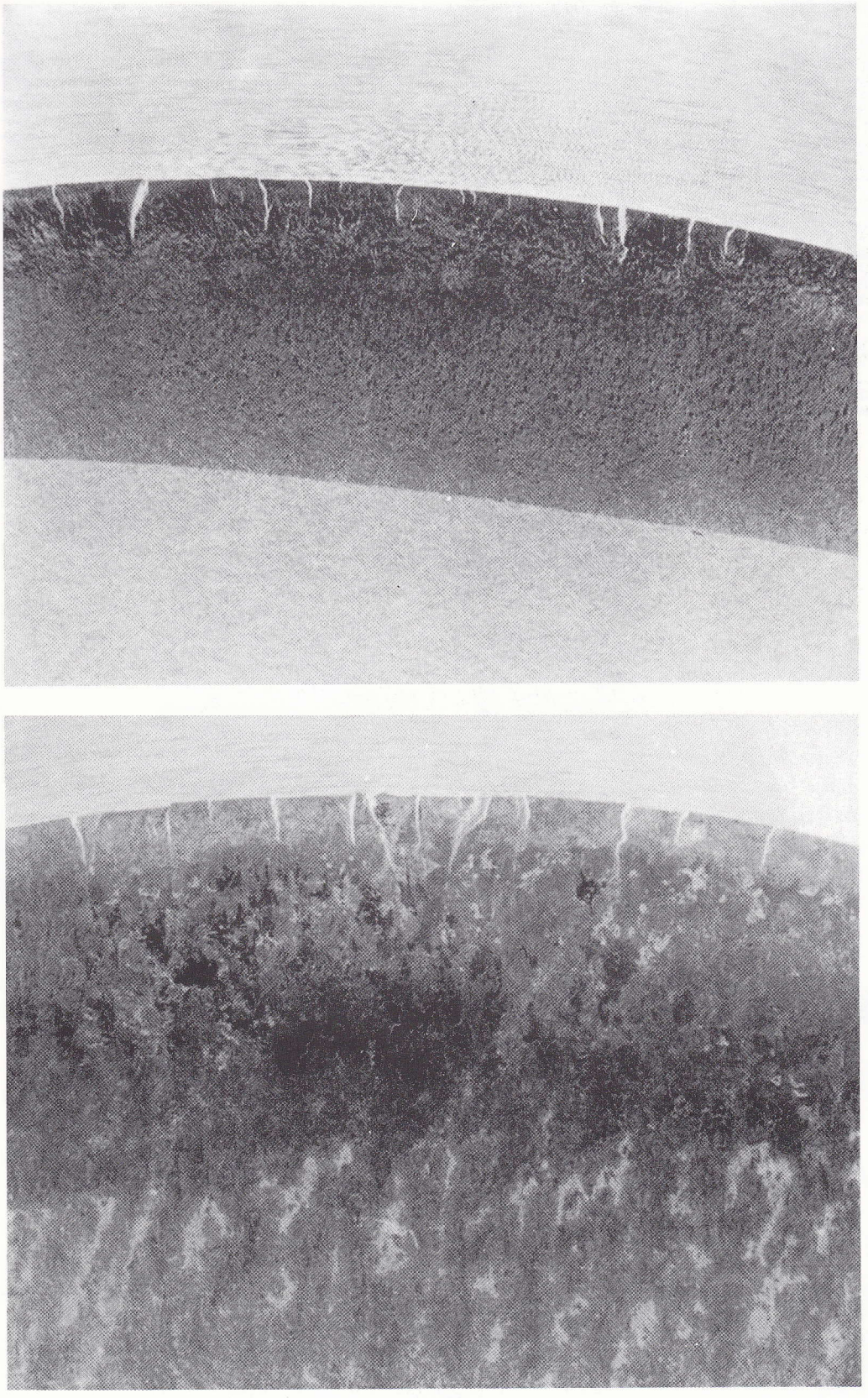

Fig. 21

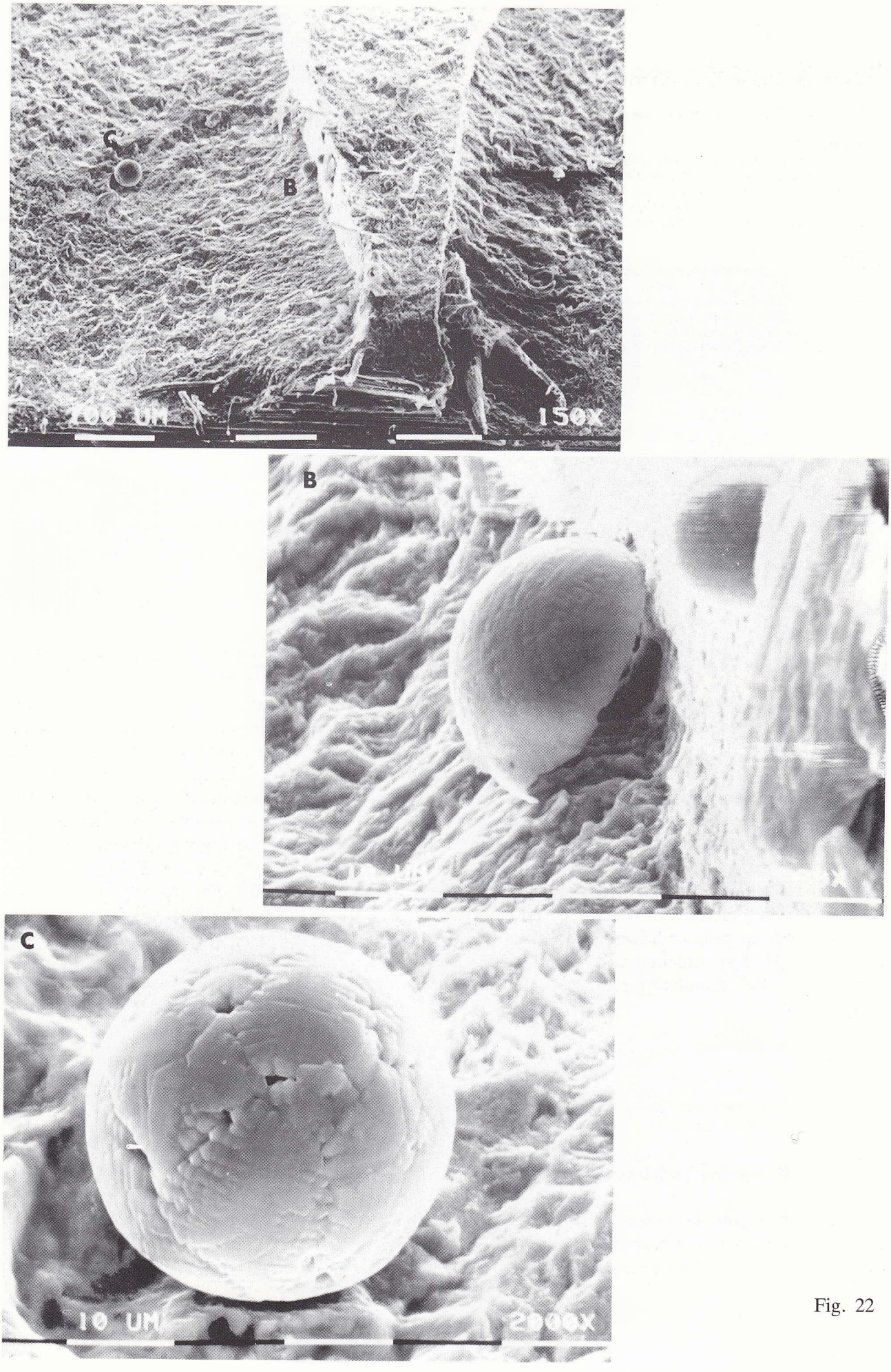

Fig. 22